

INVESTIGATION OF THE EFFECTS OF DEFORMATION TWINNING ON THE DUCTILITY OF MAGNESIUM ALLOYS

P. Cizek and M.R. Barnett

INTRODUCTION

Compression along the c-axis of the HCP unit cell leads to the least ductility in Mg single crystals. This makes cold thinning operations of Mg sheet products, characterised by strong basal textures (Fig. 1), very difficult.

C-axis contraction can be accommodated by $\langle c+a \rangle$ slip and $\{10\text{-}11\}$ “compression” twinning. $\{10\text{-}11\}$ - $\{10\text{-}12\}$ double twin formation is also possible. The aim of the work is to study the compression twin formation mechanisms and their effects on the ductility in Mg alloy polycrystals.

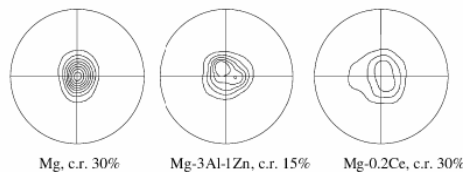


Fig. 1. Examples of the basal plane pole figures obtained from EBSD data after cold rolling. Intensity levels: 2,4,6...(times random).

EXPERIMENTAL

AZ31 (3wt.%Al-1%Zn), ZK60 (6%Zn-0.5%Zr) and ZM20 (2%Zn-0.5%Mn) alloys were used in a form of extruded bars with c-axis distributed perpendicular to the extrusion direction (Fig. 2). Tensile and compression tests were performed, along and perpendicular to the extruded bar axis respectively, at room temperature using a strain rate of 0.01 s^{-1} . EBSD was used for the microstructural study and constitutive modelling was performed to rationalise the experimental findings.

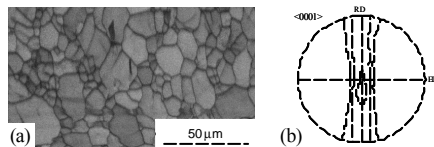


Fig. 2. Microstructure and a basal pole figure (levels: 1,2,4) for the AZ31 commercial alloy extruded bar (extrusion direction is horizontal).

RESULTS

Formation of several compression $\{10\text{-}11\}$ twin variants, characterised by the misorientation $56^\circ \langle 1\text{-}210 \rangle$, was systematically observed within the deformed grains (Fig. 3).

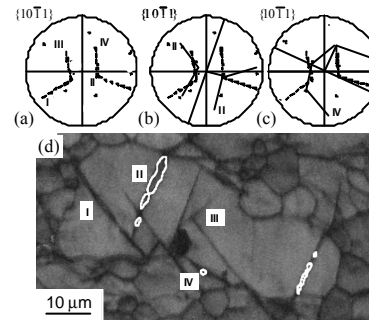


Fig. 3. EBSD analysis of $\{10\text{-}11\}$ twins in the AZ31 sample tested in tension: (a) $\{10\text{-}11\}$ matrix pole figure showing the poles that correspond to the twin HV traces; (b),(c) Pole figures for the II and IV twins respectively; (d) Kikuchi band contrast map with $\{10\text{-}11\}$ twin boundaries in white (tensile axis (TA) is horizontal).

Twin segments with misorientations about $38^\circ \langle 1\text{-}210 \rangle$, consistent with $\{10\text{-}11\}$ - $\{10\text{-}12\}$ double twinning, were also observed and they became more prevalent with increasing strain (Fig. 4). It can be seen from the above figure that the double twin reorientation leaves the basal plane in a position significantly more favourable for slip under continued loading compared to the parent grain.

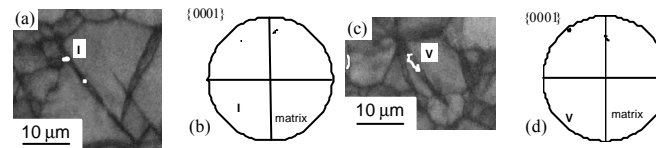


Fig. 4. EBSD analysis of $\{10\text{-}11\}$ - $\{10\text{-}12\}$ double twins in the AZ31 sample tested in tension: (a),(c) Kikuchi band contrast maps with double twin boundaries in white; (b),(d) Basal pole figures showing that the twin basal planes are favourably aligned for slip (TA is horizontal).

Tensile specimens displayed ductile failure with voids forming along the shear zones (bands) containing compression twins and double twins (Fig. 5).

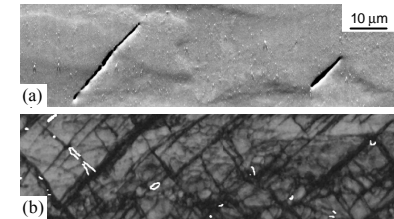


Fig. 5. The ZK60 sample tested in tension to failure: (a) Secondary electron image showing voids; (b) EBSD Kikuchi band contrast map showing shear zones and double twin boundaries in white.

A constitutive model based on double twinning has been developed. Assuming “soft” double twins, the model is able to predict the onset of the observed macroscopic work softening (Fig. 6), which eventually leads to strain localization and failure. It also suggests a role of twinning in decreasing the uniform elongation in tension.

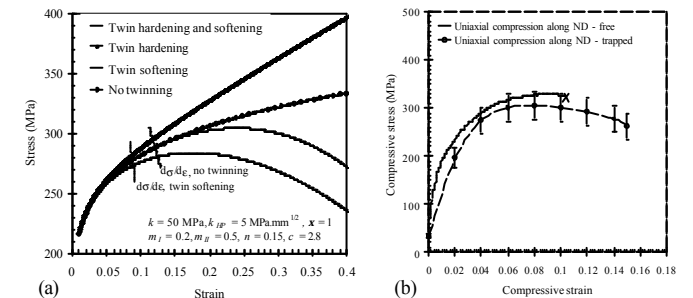


Fig. 6. (a) Predicted effect of twin hardening and softening on the overall flow behaviour; (b) Experimentally obtained flow curves for the compressed AZ31 specimen showing work softening.

CONCLUSIONS

The double twinning is expected to decrease the uniform elongation and can also account for early shear failure.